Ester-Aroyl-S,N-Ketene Acetals with Solid-State Luminescence: AIEgens from Sequential Three-Component Desymmetrization

Yannic Hartmann, Abdelouahad El Abbassi, Bernhard Mayer, Ute Resch-Genger and Thomas J. J. Müller

ChemEurJ

Research Article
doi.org/10.1002/chem.202502071

Chemistry Europe
European Chemical Societies Publishing

www.chemeurj.org

Ester-Aroyl-S,N-Ketene Acetals with Solid-State Luminescence: AIEgens from Sequential Three-Component Desymmetrization

Yannic Hartmann,[a] Abdelouahad El Abbassi,[b] Bernhard Mayer,[a] Ute Resch-Genger,*[b] and Thomas J. J. Müller*[a]

Dedicated to Prof. Dr. Jörg Pietruszka on the occasion of his 60th birthday

Di(hetero)aroyl dichlorides are desymmetrized upon sequential reaction with alcohols and 2-methyl *N*-benzyl thiazolium salts within the course of a one-pot three-component reaction yielding ester-substituted aroyl-*S*,*N*-ketene acetals under mild conditions in good yields. A prerequisite for the concise one-pot process is the different nucleophilicity of the alcohols and in situ generated *S*,*N*-ketene acetals. The resulting compounds are merocyanines with dominant charge-transfer absorption bands which are fluorescent in the solid state, but not in solution. In water/ethanol solvent mixtures of increasing water content, the water-insoluble dyes display typical aggregation-induced emission (AIE) characteristics. The water fraction inducing AIE as well as the emission color, and fluorescence quantum yield (Φ_f) of the aggregated dyes can be controlled by the alcohol part of the ester moiety. Encapsulation into polystyrene nanoparticles can lead to a considerable increase of the fluorescence quantum yield Φ_f to 30% as shown for a representatively chosen dye revealing the highest Φ_f of 11% within the dye series in the water/ethanol mixtures and enabling the usage of these dyes as fluorescent reporters in aqueous environments.

1. Introduction

The design of functional chromophores[1] presents the basis for many phototonic applications of organic fluorophores and molecular electronics.[2] Examples range from dye sensitizers in organic photovoltaics[3,4] and emitters in organic light-emitting diodes,[5–8] to semiconducting molecular charge transport materials in devices switchable by electric current[9,10] luminophores for sensing and bioimaging studies,[11–15] to photoredox catalysts opening new alleys in photoreactivity.[16–18] Approaches to rapidly access functional chromophores began with combinatorial syntheses[19–21] and have inspired novel synthetic strategies.[22–25] A particularly promising reactivity-based concept is one-pot methodologies, such as multicomponent reactions (MCR) – performed in a domino, sequential, or consecutive fashion[26] that enable a rational design of libraries of compounds with a large structural and functional diversity.[27] Over the past two decades, such MCRs have been established as a powerful synthetic tool to access numerous classes of functional chromophores.[28—34]

Among emissive materials, emission upon induced aggregation, also known as aggregation-induced emission (AIE),[30,33,35–39] is increasingly popular as it can be widely employed to overcome the loss of photonic properties often seen in the solid state as a consequence of aggregation-caused quenching (ACQ). AIEgens, that is, luminophores that reveal a turned-on luminescence upon aggregation, can be meanwhile accessed by MCR strategies,[40] as has been demonstrated by us for several dye families. In recent years, we have established a facile chromogenic approach to aroyl-*S*,*N*-ketene acetals, which present relatively small push-pull π-conjugated systems that typically show AIE behavior and a broad color tunability.[41,42] This concept has been meanwhile, expanded to bi- and even multichromophore AIE systems, which can be employed, e.g., as dual emissive AIE polarity sensors.[43] To further expand the methodological scope of the condensation synthesis of aroyl-*S*,*N*-ketene acetals and enhance functional diversity, we focus here on ester-substituted aroyl-*S*,*N*-ketene acetal chromophores accessed by one-pot reactions by the desymmetrization of diaroyl dichlorides (Scheme 1).

While symmetric acylations of terephthaloyl chloride are common, only very few examples for desymmetrization with two different nucleophiles have been reported so far.[44–46] More common are stepwise desymmetrizations of terephthaloyl chloride, for instance, by monoacylation and intermediate workup.[47] However, due to the pronounced reactivity of *S*,*N*-ketene

[a] Y. Hartmann, Dr. B. Mayer, Prof. Dr. T. J. J. Müller
Institut für Organische Chemie und Makromolekulare Chemie, Heinrich-Heine-Universität Düsseldorf, Universitätsstraße 1, D-40225 Düsseldorf, Germany
E-mail: ThomasJJ.Mueller@hhu.de

[b] A. El Abbassi, Dr. U. Resch-Genger
Division Biophotonics, Bundesanstalt für Materialforschung und -prüfung (BAM), Richard-Willstätter-Straße 11, D-12489 Berlin, Germany
E-mail: ute.resch@bam.de

Yannic Hartmann and Abdelouahad El Abbassi contributed equally to this work.

Supporting information for this article is available on the WWW under https://doi.org/10.1002/chem.202502071

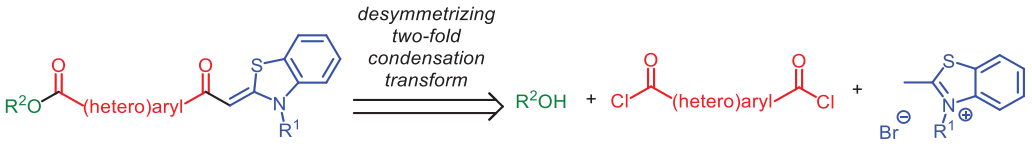

Scheme 1. Retrosynthetic analysis of ester-substituted aroyl-*S*,*N*-ketene acetals.

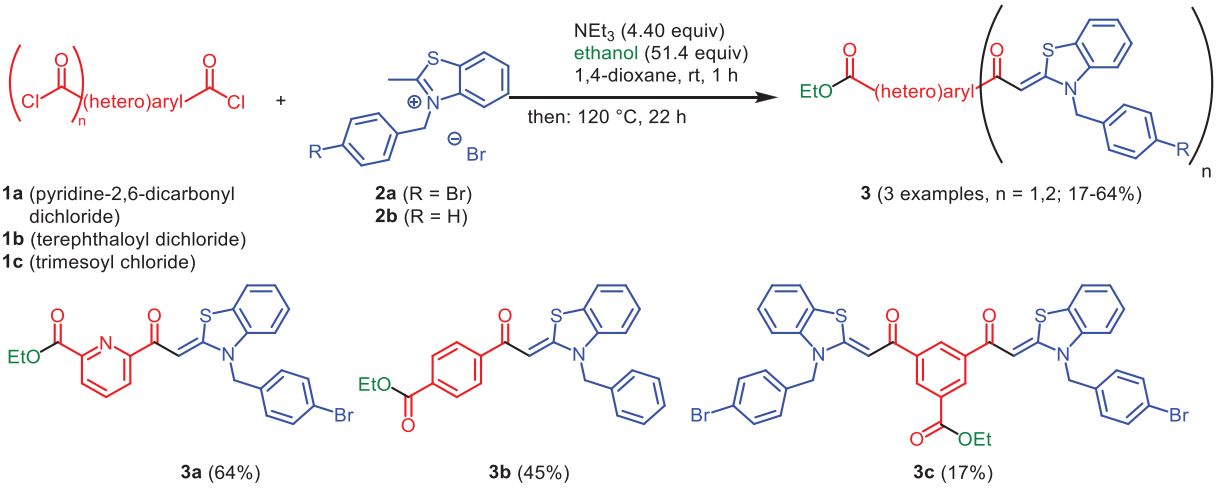

Scheme 2. Domino reaction of bis- and trisaroyl chlorides **1** and 3-benzyl-2-methylbenzo[*d*]thiazol-3-ium bromides **2** in dioxane and ethanol forming carboxyethyl-substituted aroyl-*S*,*N*-ketene acetals **3**.

acetals,[48] which are the actual nucleophiles in the synthesis of aroyl-*S*,*N*-ketene acetals, we envisioned a tunable transformation of diaroyl dichlorides. Herein, we report the methodological development of a desymmetrizing twofold acylation of diaroyl dichlorides with 3-benzyl-2-methylbenzo[*d*]thiazol-3-ium (as precursors to *S*,*N*-ketene acetals) and alcohols for accessing ester-substituted aroyl-*S*,*N*-ketene acetals in a sequential three-component reaction. Almost all dyes of the resulting dye library are emissive in the solid state and reveal AIE behavior, as shown by spectroscopic studies in solution and in the solid state with a substitution pattern-dependent dependence of the aggregation behavior, emission color, and fluorescence quantum yield (Φ_f).

2. Results and Discussion

2.1. Synthesis

The diversity-oriented character of the aroyl-*S*,*N*-ketene acetal synthesis can be addressed by a selective desymmetrization of diaroyl dichlorides. While one acid chloride functionality serves to establish the underlying aroyl-*S*,*N*-ketene acetal chromophore, the second acid chloride unit allows for acylation of the heteroatom nucleophiles. As seen in the initial studies, acceptor substituents, such as nitriles and nitro groups, conjugated with the carbonyl group of the respective chromophores, cause a red-shifted absorption and AIE. The synthesis of esters, which are weaker acceptors, by Einhorn-type acylation[49] promises the easy conversion of acid chlorides with variable alcohols. Therefore, the consecutive one-pot synthesis of ester-substituted aroyl-*S*,*N*-ketene acetals represents an attractive synthetic strategy for assessing novel dyes with interesting spectroscopic properties in solution and in the solid state.

First, we examined the standard conditions for aroyl-*S*,*N*-ketene acetal synthesis, [41,42], that is, by employing dioxane as a solvent with a 50–70-fold excess of ethanol and triethylamine as a base, the latter in amounts slightly exceeding a stoichiometric ratio, with pyridine-2,6-dicarbonyl dichloride (**1a**), terephthaloyl dichloride (**1b**), or trimesoyl chloride (**1c**) and 3-(4-bromobenzyl)-2-methylbenzo[d]thiazol-3-ium bromide (**2a**) or 3-benzyl-2-methylbenzo[d]thiazol-3-ium bromide (**2b**). The corresponding carboxyethyl-substituted aroyl-*S*,*N*-ketene acetals **3** were obtained in moderate to good yield under unoptimized conditions (Scheme 2) after purification by flash chromatography on silica gel.

The remarkable selectivity of the desymmetrization, leading to the formation of carboxyethyl-substituted aroyl-*S*,*N*-ketene acetals **3**, is ascribed to the significant differences in the nucleophilicity of ethanol and the *S*,*N*-ketene acetal, which is in situ formed by deprotonation of the 3-benzyl-2-methylbenzo[*d*]thiazol-3-ium salts **2**. Although, no nucleophilicity parameter *N* for this specific *S*,*N*-ketene acetal has been reported to date, it can be estimated by employing Mayr's nucleophilicity scales[50–52] to the ketene acetals (N = 9–13), enamines (N = 10–16), cyclic *N*,*N*-ketene acetals (N = 18–20),[53,54] and the deoxy-Breslow intermediate (N = 15.6).[55] This reveals that, the nucleophilicity of the presumed *S*,*N*-ketene acetal significantly exceeds those of ethanol (N = 7.4) and other alcohols. However, the employed base triethylamine is more nucleophilic (N = 17.30 in dichloromethane; N = 17.10 in acetonitrile).[56] Therefore, a scenario where the first intermediate formed from bisaroyl chlorides

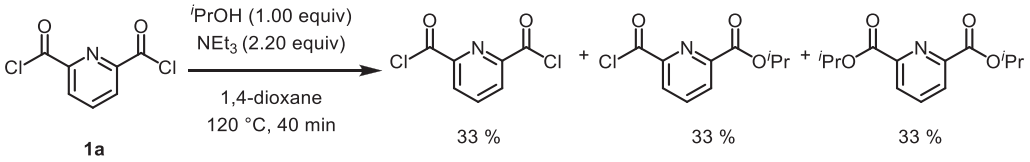

Scheme 3. Equistoichiometric acylation of isopropanol with pyridine-2,6-dicarbonyl dichloride (**1a**) and the observed product mixture.

is an acylammonium species, like in an Einhorn acylation,[49] becomes very plausible. Transferring these conditions to isopropanol as the alcohol (excess of 25–50 equiv as in Scheme 1) in a test reaction with pyridine-2,6-dicarbonyl dichloride (**1a**) and 3-(4-bromobenzyl)-2-methylbenzo[*d*]thiazol-3-ium bromide (**2a**) reveals significantly reduced yields of the corresponding ester-substituted aroyl-*S*,*N*-ketene acetal **3i**. In addition, a substantial amount of the corresponding bis(aroyl-*S*,*N*-ketene acetal) is formed (see Supporting Information, chapter 2.4). Therefore, the domino process, that is, all reagents are present at the outset of the process, was discarded for a general desymmetrizing acylation one-pot strategy.

For the synthesis of the ester-substituted aroyl-*S*,*N*-ketene acetals with sequential reaction control, the esterification of the aryl diacid dichloride should occur in the first step and the nucleophilic attack of the more reactive *S*,*N*-ketene acetal, generated in situ, in the second step. Reversing the reaction, that is, initial formation of the aroyl-*S*,*N*-ketene acetal scaffold followed by esterification, did not lead to product formation. A test reaction and Cuilleron's observations[47] confirm that even the equimolar addition of alcohol to the acid chloride leads to the formation of the corresponding diester (Scheme 3).

Therefore, for the complete conversion of the diaroyl chloride, in agreement with the literature,[47] an excess of 1.5 equivalents of alcohol per diaroyl chloride is required, since the formed diester does not compete with the generated monochloride. Consequently, we employed this ratio to optimize the reaction of the substrates **1a**, **2a**, and isopropanol to give product **3i**. However, a reaction temperature of 120 °C does not furnish higher yields of the ester-substituted aroyl-*S*,*N*-ketene acetal **3i** (see Supporting Information, chapter 2.5). The observed red coloration of the reaction solution after addition of benzothiazolium salt **2a** at elevated temperatures, even in the absence of diaroyl dichloride **1a**, very likely accounts for the formation of undefined oligomerization products.[57] Hence, the twofold desymmetrizing acylation of diaroyl dichlorides must be sequentially performed at room temperature rather than at elevated temperature to suppress side reactions. As a consequence, the initial protocol for aroyl-*S*,*N*-ketene acetal formation[41,42] was modified, circumventing the usage of alcohols as cosolvents in the presence of benzothiazolium salts, and the reaction was conducted at room temperature in 1,4-dioxane as the sole solvent.[58] Subsequently, upon sequential reaction of di(hetero)aroyl dichlorides **1** and alcohols **4** in the presence of triethylamine as a base in 1,4-dioxane or dichloromethane as a solvent at room temperature for 45 minutes followed by addition of 3-(4-bromobenzyl)-2-methylbenzo[*d*]thiazol-3-ium bromide (**2a**) and reaction at room temperature for 14 minutes, 16 ester-substituted aroyl-*S*,*N*-ketene acetals **3** could be obtained in yields of 24–85% after purification (Scheme 4).

This sequential approach allows for the usage of a broad variation of primary and secondary alcohols as well as phenol, with the latter, however, providing a lower yield. The critical factor for a high conversion and the successful desymmetrization of di(hetero)aroyl dichlorides is the solubility of the substrates in the applied solvent system. Tests show that 1,4-dioxane or dichloromethane are the optimum solvents. Tertiary alcohols, such as *tert*-butanol failed to give the targeted ester-substituted aroyl-*S*,*N*-ketene acetals **3** under standard conditions. However, switching to pyridine as an acylation mediator with a lower pK_a in the esterification step using dichloromethane *as* a solvent and a reaction temperature of 50 °C leads to the formation of ester-substituted aroyl-*S*,*N*-ketene acetal **3s** after 17 hours. Thereby, compound **3s** was obtained in a yield of 56% after chromatographic purification and trituration (Scheme 5).

While trimesoyl chloride (**1c**) reacts in the domino sequence (vide supra) to give the carboxylethyl-substituted bis(aroyl-*S*,*N*-ketene acetal) **3c** in a poor yield, after adjusting the stoichiometry, the biscarboxylethyl-substituted aroyl-*S*,*N*-ketene acetal **3t** could be obtained by the sequential transformation in hexane in a good yield after chromatography and trituration (Scheme 6).

For reversing the order of the acylation of the nucleophiles, we next assessed a short reaction time of diaroyl dichloride **1b** (in a twofold excess) with 3-(4-bromobenzyl)-2-methylbenzo[d]thiazol-3-ium bromide (**2a**) in dichloromethane in the presence of triethylamine at room temperature. Interestingly, the acid chloride-substituted aroyl-*S*,*N*-ketene acetal **5** can be obtained in an excellent yield after purification (Scheme 7).

With the acid chloride-substituted aroyl-*S*,*N*-ketene acetal **5** at hand, also more complex substrates such as the steroid alcohol dihydrotestosterone (**4k**) can be acylated in the presence of *N*,*N*-dimethylamino pyridine (DMAP) to give ester-substituted aroyl-*S*,*N*-ketene acetal **3u** in a moderate yield (Scheme 8).

Finally, the sequential desymmetrizing acylation of diaroyl dichloride **1b** can be examined in a one-pot reaction using 3-(4-bromobenzyl)-2-methylbenzo[*d*]thiazol-3-ium bromide (**2a**) and employing diethylamine as the second nucleophile. This provided amide-substituted aroyl-*S*,*N*-ketene acetal **6** in good yield after chromatography and trituration (Scheme 9).

The structure of the ester-, carbonyl chloride-, and amide-substituted aroyl-*S*,*N*-ketene acetals **3**, **5**, and **6** was unambiguously assigned via extensive NMR studies, mass spectrometry, and IR spectroscopy, and its molecular composition by combustion analysis.

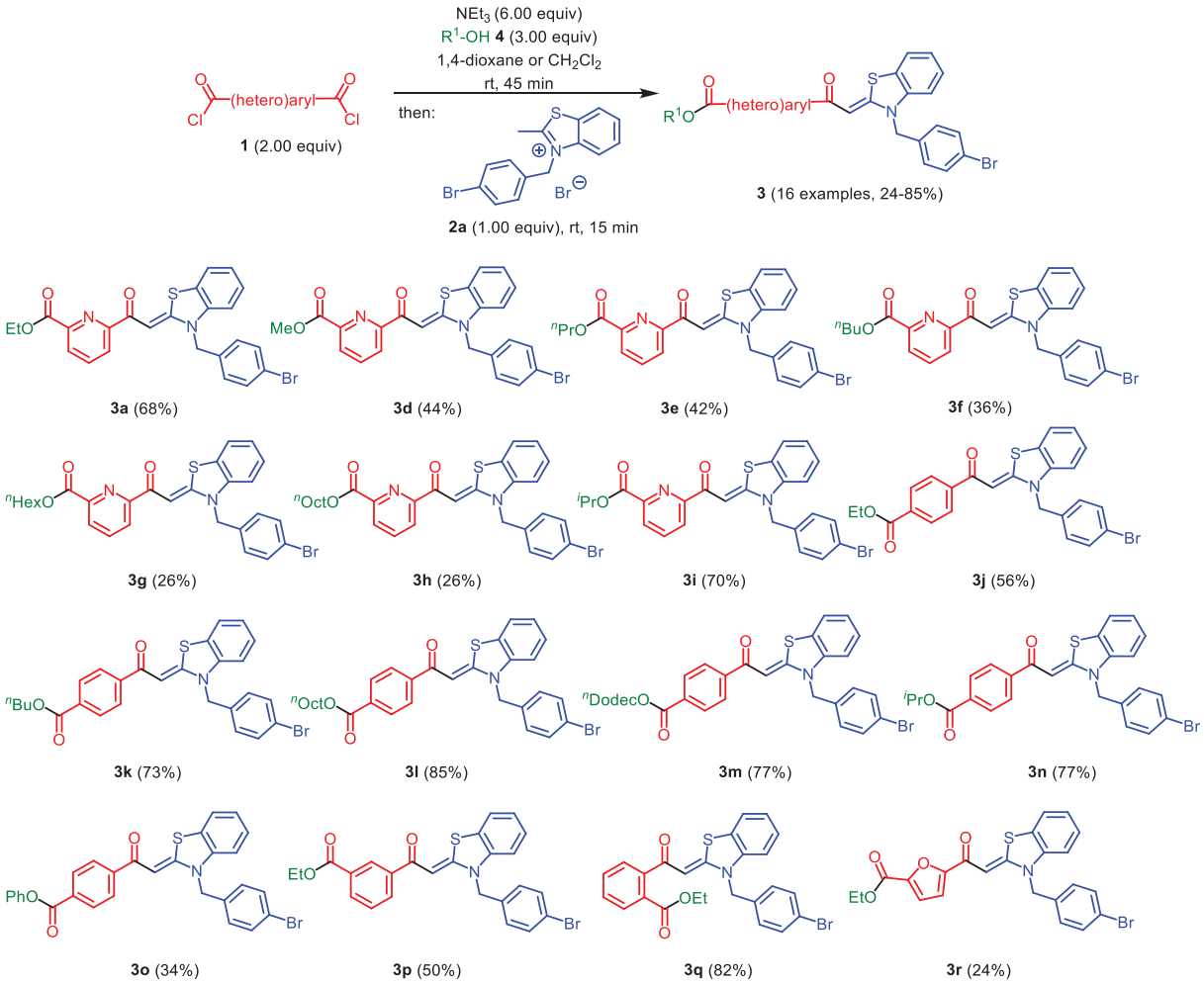

Scheme 4. Sequential desymmetrization of di(hetero)aroyl dichlorides **1** with alcohols **4** and 3-(4-bromobenzyl)-2-methylbenzo[d]thiazol-3-ium bromide (**2a**) in 1,4-dioxane or dichloromethane to give ester-substituted aroyl-*S*,*N*-ketene acetals **3**.

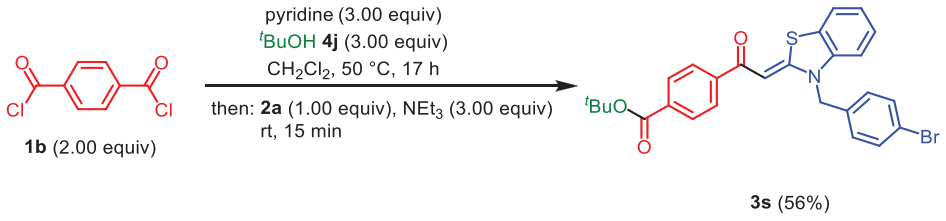

Scheme 5. Consecutive one-pot synthesis of *tert*-butyl carboxyl-substituted aroyl-*S*,*N*-ketene acetal **3s** in the presence of pyridine in dichloromethane.

2.2. Photophysical Properties and Electronic Structure

Absorption and emission spectroscopy. Except for dye **3p**, all compounds **3** display an intense luminescence in the solid state upon excitation with a hand-held UV lamp (λ_{exc} = 365 nm), but in solution no emission could be detected by the naked eye. Spectrofluorometric measurements in ethanol and THF revealed only a very weak emission with Φ_F values below 1%. Next,

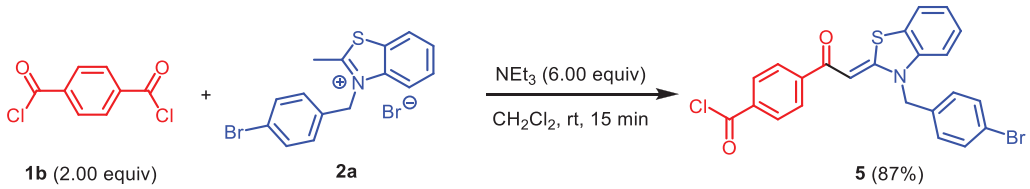

Scheme 7. Synthesis of acid chloride-substituted aroyl-*S*,*N*-ketene acetal **5** in dichloromethane.

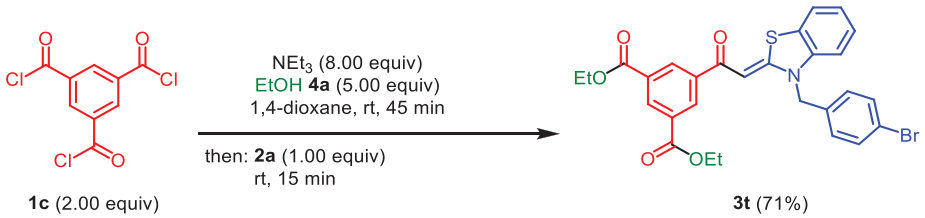

Scheme 6. Sequential one-pot synthesis of biscarboxylethyl-substituted aroyl-*S*,*N*-ketene acetal **3t** in 1,4-dioxane.

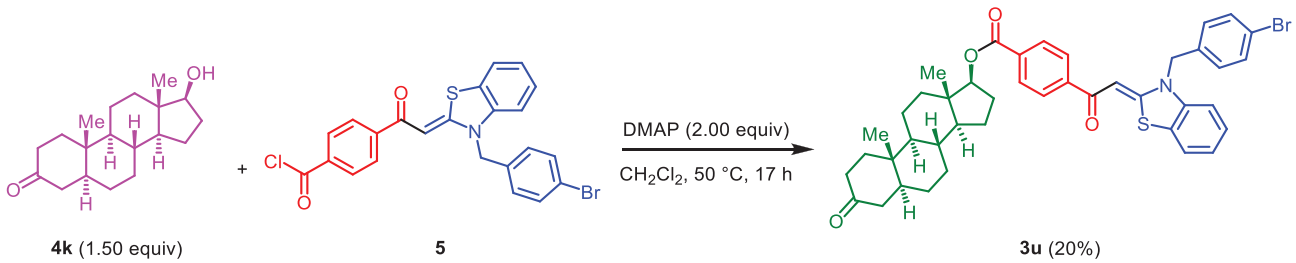

Scheme 8. Einhorn acylation of dihydrotestosterone (**4k**) with acid chloride-substituted aroyl-*S*,*N*-ketene acetal **5**.

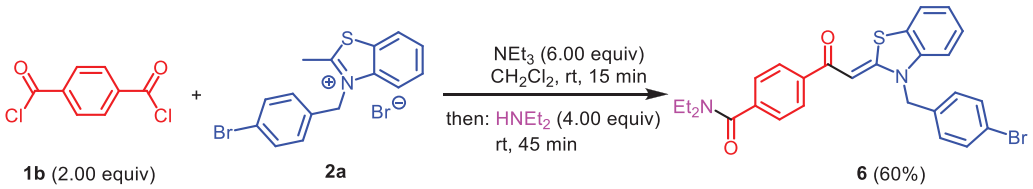

Scheme 9. Sequential one-pot synthesis of amide-substituted aroyl-*S*,*N*-ketene acetal **6**.

we investigated the spectroscopic properties of compound **3** in ethanolic solution at room temperature and also determined the emission spectra in the solid state (Table 1).

First, the absorption spectra of the consanguineous series of ester-substituted terephthaloyl aroyl-*S*,*N*-ketene acetals **3j-o,s** were compared (Figure 1A). Expectedly, the broad absorption bands of the aroyl-*S*,*N*-ketene acetal chromophore with molar extinction coefficients between 28 400 and 58 400 $L \cdot mol^{-1} \cdot cm^{-1}$ are located within a narrow wavelength range between 396 and 405 nm. Similarly, the consanguineous series of various alkyl ester-substituted 2,6-pyridindioyl-*S*,*N*-ketene acetals with unit **3a,d-i** displays the same absorption characteristics (see Supporting Information, Figure S47).

More distinct are the solid-state emission spectra of ester-substituted terephthaloyl aroyl-*S*,*N*-ketene acetals **3j-o,s** (Figure 1B) with the emission maxima being located between 500 and 568 nm. While the dye absorption characteristics in solution are mainly influenced by the molecules´ electronic properties, the solid-state fluorescence is also affected by the crystal packing and intermolecular interactions.[59,60] For instance, long-chain alkoxy groups lead to hypsochromically shifted emission bands located at $\lambda_{max,em} = 500$ nm (**3l**) and 501 nm (**3 m**), respectively. Also, the emission maximum of phenyl ester **3o** at 506 nm is located in this wavelength range. The derivatives with shorter primary alkoxy chains display red-shifted emission bands at 538 nm (**3j**) and 533 nm (**3k**), respectively. However, the emission band of the *n*-butyl ester presents superpositions of several bands between 477 and 570 nm, suggesting the presence of several conformers in the solid state. Secondary and tertiary alkoxy substituents clearly cause a red shift in emission compared to primary alkoxy moieties. While the *tert*-butyl ester derivative **3s** shows an emission maximum at 547 nm, the maximum of the isopropyl ester dye **3n** is bathochromically shifted to 568 nm. The related 2,6-pyridindioyl derivatives **3a,d-l** are not linear but kinked chromophores. Therefore, the emission bands appear around 500 nm. Yet, the *n*-butyl derivative (**3f**) displays an additional red-shifted band at 614 nm (see Supporting Information, Figure S52).

Next, we investigated the influence of the (hetero)aroyl moiety on the electronic spectra for a series of consanguineous ethyl esters (Figure 2). The absorption maxima of 2,6-pyridinoyl (**3a**), terephthaloyl (**3j**), and 2,5-furoyl (**3r**) bridged chromophores at 401, 397, and 405 nm, respectively (Figure 2A), are the most red-shifted. In contrast, the absorption maximum of the phthaloyl derivative **3q** is hypsochromically shifted to 367 nm. This is ascribed to conformational strain that reduces the overlap of the orbitals on the side of the acceptor moiety, albeit the ester is in conjugation to the ketone. Due to *meta*-substitution, the absorption maximum of trimesoyl derivative **3t** experiences a slight hypsochromic shift to 391 nm. This underlines that the nature of bridging aroyl moieties exerts a more distinct influence on the longest wavelength absorption bands in solution compared to the nature of the alkoxy moiety. In addition, the unperturbed conjugation pathway of the ester moiety and the ketone leads to a significant increase of the molar extinction coefficients of the terephthaloyl (**3j**, $\varepsilon = 58\ 400\ L \cdot mol^{-1} \cdot cm^{-1}$) and

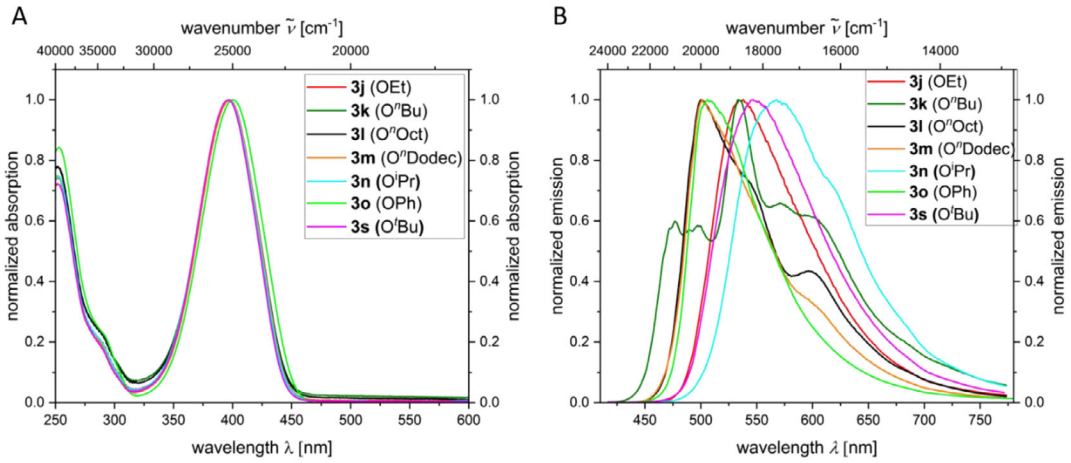

Figure 1. A) Normalized absorption spectra of compounds **3j-o,s** (T = 298 K, c(**3**) = 10^{-5} M) with varying alkoxy components in ethanol. B) Normalized solid-state emission spectra of selected compounds **3j-o,s** with varying alkoxy components (T = 298 K, λ_{exc} = $\lambda_{max,abs}$).

Table 1. Selected spectroscopic data of ester-substituted (hetero)aroyl-*S,N*-ketene acetals **3** (most intense emission peaks are in bold face) in ethanolic solution (absorption data) and in the solid state (emission data). The ethanolic dye solutions are nonemissive.

Compound[b]	$\lambda_{max,abs}$ [nm] [ε [L·mol^{-1}·cm^{-1}]][a]	$\lambda_{max,em}$ [nm][b] [Φ_f][c]
3a	401 (36 700)	496 (0.09)
3b	397 (33 900)	490, 497 (0.11)
3c	399 (72 000)	511 (0.01)
3d	400 (32 800)	498 (0.06)
3e	401 (26 900)	496 (0.08)
3f	401 (30 300)	497, 516, 614 (0.09)
3g	401 (41 100)	497 (0.07)
3h	401 (31 000)	491 (0.03)
3i	402 (31 000)	500 (0.03)
3j	397 (58 400)	538 (0.05)
3k	397 (36 900)	477, 490, 497, **533**, 570 (0.07)
3l	397 (42 200)	500, 592 (0.12)
3m	397 (37 100)	501 (0.09)
3n	397 (37 300)	568 (0.05)
3o	400 (28 400)	506 (0.09)
3p	386 (31 500)	—[d]
3q	367 (39 800)	448 (0.09)
3r	405 (69 300), 283 (39 100)	531, 592 (0.02)
3s	396 (52 700)	547 (0.13)
3t	391 (38 600)	511 (0.09)
3u	396 (19 300)	567 (0.02)

[a] Recorded in ethanol, T = 298 K, c(**3**) = 10^{-5} M.
[b] Recorded in the solid state, λ_{exc} = $\lambda_{max,abs}$; T = 298 K.
[c] Recorded with an integrating sphere, T = 298 K.
[d] Not measured.

2,5-furoyl bridged dyes (**3r**, ε = 69 300 L · mol^{-1} · cm^{-1}) in comparison to the deconjugated, yet strongly electron-withdrawing 2,6-pyridoyl bridged system **3a** (ε = 36 700 L · mol^{-1} · cm^{-1}).

Compared to the absorption properties, the influence of the (hetero)aroyl bridge on the solid-state fluorescence is more pronounced (Figure 2B). While the strongly hypsochromically shifted maximum of the blue emission of phthaloyl derivative **3q** appears at 448 nm, 2,6-pyridinoyl bridged dye **3a** reveals a green fluorescence peaking at 496 nm, trimesoyl bridged dye **3t** luminesces with a greenish color and displays an emission maximum at 511 nm. The terephthaloyl and 2,5-furoyl derivatives **3j** and **3r** show a fluorescence at 538 and 531 nm, respectively. The latter possesses an additional low energy shoulder at 592 nm.

TD-DFT Calculations. To rationalize the electronic structure of the dye molecules, quantum chemical calculations on the DFT and TD-DFT level of theory were performed with Gaussian 16[61] choosing **3j** as a representative chromophore (see Supporting Information, Table S4). Thereby the longest wavelength absorption band was assigned to the respective electronic transitions. First, the geometry of the ground state was optimized employing the standard B3LYP hybrid functional[62–64] and the 6–31G** basis set[65] using the polarizable continuum model (PCM) with ethanol as a dipolar protic implicit dielectric medium with a dielectric constant ε = 24.85.[66] Frequency analysis was employed to verify the structure optimization. Then, the lowest energy transitions were calculated by TD-DFT calculations, again using PCM with CH_2Cl_2 as a solvent continuum (see Supporting Information, Table S4).[66] The first six calculated singlet states reproduce very well the experimentally determined absorption maxima with a deviation of ΔE = 0.014 eV for the lowest energy absorption. This lowest energy band (S_1 state) is represented by a HOMO→LUMO transition and Kohn-Sham orbitals clearly indicate a dominant charge transfer (CT) character (Figure 3).

2.3. AIE Studies with Dyes 3

Aroyl-*S,N*-ketene acetals are meanwhile well known for their excellent AIE characteristics.[41] Since dyes **3** are soluble in ethanol and insoluble in water, AIE measurements were done in water/ethanol mixtures with varied water content of up to 95%, according to a previously standardized protocol,[67] thereby

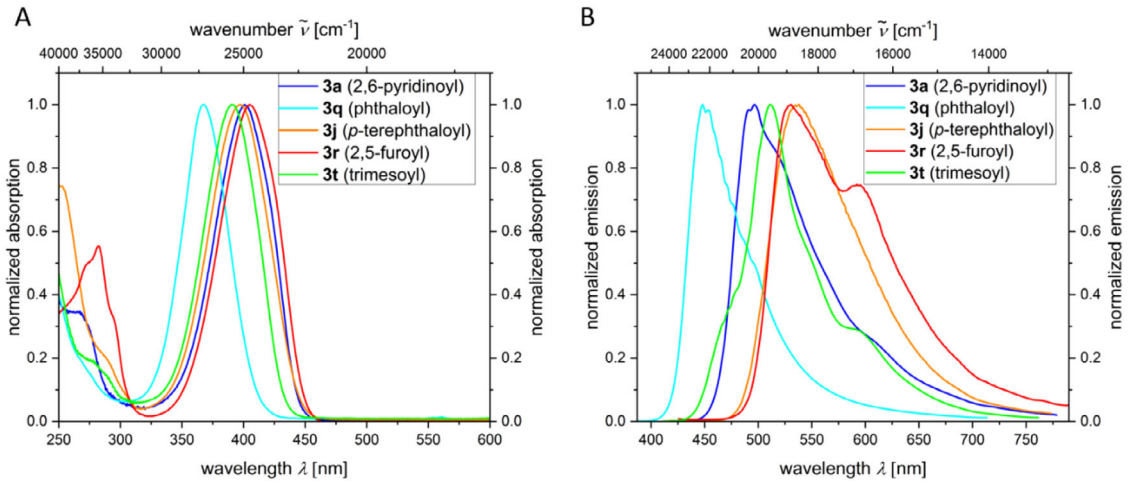

Figure 2. A) Normalized absorption spectra of selected ethyl esters **3** with varying (hetero)aroyl moieties (recorded in ethanol, $T = 298$ K, c(**3**) $= 10^{-5}$ M). B) Normalized solid-state emission spectra of selected ethyl esters **3** with varying (hetero)aroyl moieties ($T = 298$ K, $\lambda_{exc} = \lambda_{max,abs}$).

keeping the chromophore concentration constant. Dye aggregation induced by water led to fluorescence enhancement factors of more than 30. As representatively shown for dye **3j**, the solubility of the dye decreased with increasing water content of the water/ethanol mixtures. For a water content of 70%, increased aggregation occurs, accompanied by an enhancement in fluorescence intensity (Figure 4A).

At a water content of 20%, **3j** starts to weakly emit (Figure 4, top panel, left). At a water content of 90–95%, the maximum fluorescence intensity is reached, which exceeds the fluorescence at a water content of 20% by a factor of 20. The increase in fluorescence intensity is accompanied by a red shift of the emission band, that is, a color shift from green ($\lambda_{max,em} = 503$ nm) to yellowish ($\lambda_{max,em} = 539$ nm) with a simultaneous broadening of the emission band (Figure 4, top panel, right). These spectral changes are ascribed to the increased polarity of the dye and aggregate microenvironment. The maximum Φ_F of aggregated **3j** amounts to 6% (Figure 4, top panel, right). Above a water content of 90%, the fluorescence intensity starts to decrease, presumably due to precipitation of the AIEgen. For dye **3l**, containing a longer alkyl chain, that is, an octyl substituent, the water-induced aggregation and the concomitant increase of the emission already reach a maximum at a water content of 70% (Figure 4B), revealing an enhancement factor of 25. The quantum yield Φ_F amounts to 8%. As observed for **3j**, an increase in water content, and hence solvent polarity, leads to a red shift of the fluorescence, resulting in a color change of the initially green fluorescence ($\lambda_{max,em} = 509$ nm) to orange and the appearance of an additional emission maximum at 596 nm for higher water fractions. In the case of dye **3 m** bearing a dodecyl alkyl chain, strong aggregation already starts at a water content of 60%, and the maximum fluorescence intensity is reached at a water content of 70%. With a Φ_F of 11%, dye **3 m** displays the highest fluorescence quantum yield of the three dyes. As observed for alkyl esters **3j** and **3l**, the broad, more or less unstructured emission band of **3 m** is also red shifted with increasing solvent polarity, accompanied by a change in emission color from green to yellow (Figure 4C). As observed for the other two

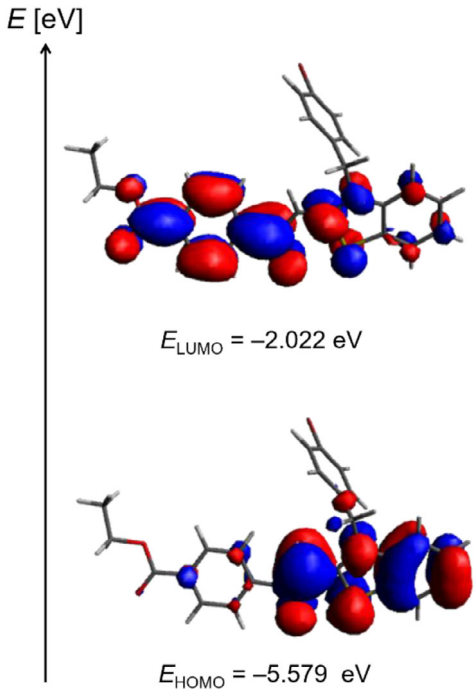

Figure 3. Kohn-Sham frontier molecular orbitals of dye **3j** calculated with TD-DFT (B3LYP/6–31G**; using C-PCM for the solvent ethanol).

dyes, the aggregates formed at water contents as high as 95% slowly begin to precipitate after a few hours. A comparison of the AIE behavior of the ethyl (**3j**), octyl (**3l**), and dodecyl (**3 m**) ester-substituted aroyl-*S*,*N*-ketene acetals reveals relatively similar fluorescence features of the aggregated dyes, with the length of the alkyl ester chain systematically shifting the water fraction, at which maximum fluorescence is observed, from 80% (**3j**) and 70% (**3l**) to 60% (**3 m**) and enhancing the resulting Φ_f from 6% (**3j**) and 8% (**3l**) to 11% (**3 m**). Apparently, an increasing length of the alkyl ester chain of the dyes favors dye aggregation already at a lower water fraction and leads to slightly higher Φ.

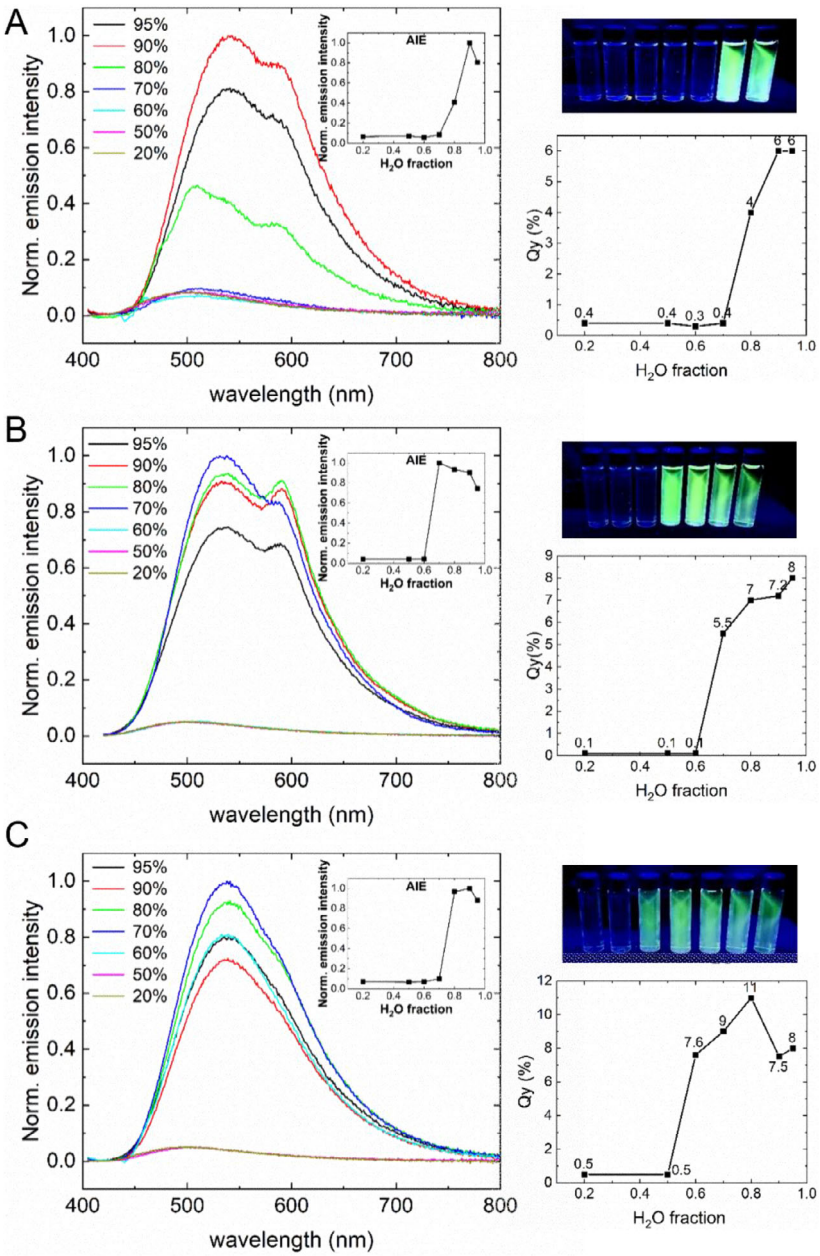

Figure 4. AIE behavior of dyes **3j** (A), **3l** (B), and **3 m** (C) in water/ethanol mixtures of increasing water content. Left column: Normalized spectrally corrected fluorescence emission spectra recorded in water/ethanol mixtures (T = 298 K, c(**3**) = 10^{-6} M), excitation at the absorption maximum (λ_{exc} = $\lambda_{max,abs}$). The spectrally corrected emission spectra are normalized to the maximum emission intensity observed at the highest water fraction where the dye is still emissive. Insets: Normalized fluorescence intensity at the emission maximum plotted as a function of the water fraction of the water/ethanol mixtures, illustrating the AIE trends. Right column: The top panels show representative photographs of the dye solutions under 365 nm illumination, demonstrating the enhanced emission upon aggregation and the emission color. The bottom panels reveal the fluorescence quantum yields (Φ_f) as a function of the water fraction of the water/ethanol mixtures, confirming the increase in emission efficiency upon water-induced aggregation.

A comparison of the dyes **3n** (isopropyl ester), **3o** (phenyl ester), and **3s** (*tert*-butyl ester) reveals slightly lower Φ_f values for the maximally achievable emission of the aggregated dyes for water fractions between 80% and 95% with only small polarity-induced spectral shifts in emission with increasing water content (see Supporting Information, Figures S58–S60). The trimesoyl dye **3t** displays a Φ_f of 8% at a very high water fraction of 95%. The appearance of multiple shoulders in the emission spectra suggests the presence of multiple emissive conformers in the aggregates (see Supporting Information, Figure S61). In contrast, the highly unipolar dihydrotestosterone ester dye **3u** exhibits a maximum Φ_f of 4% reached at a water fraction of 80% and displays a redshift in emission for water fractions between 40% and 60%, followed by a blue shift of the emission maximum at a higher water fraction (see Supporting Information, Figure S62). Diethylamide derivative **6**, which possesses a slightly blue-shifted absorption band in ethanol ($\lambda_{max,abs}$ = 389 nm; ε = 35 900 L·mol^{-1}·cm^{-1}) and a solid-state emission maximum at 535 nm with a Φ_f of 12%, displays a higher Φ_f of 8% at a water content of 90% and no spectral shifts in water/ethanol

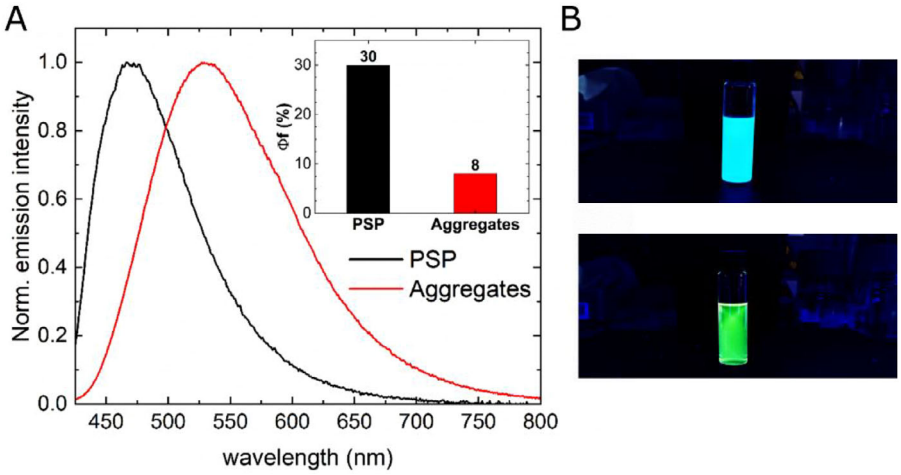

Figure 5. A) Normalized spectrally corrected fluorescence emission spectra of dye **3l** in the aggregated state (red, 90% H_2O in THF) and encapsulated in 200 nm carboxylated PSPs (black). The inset shows the corresponding Φ_f values. B) Representative photographs of dye **3l** in PSPs (top) and in THF/H_2O (10/90) mixture (bottom) under the hand-held UV-lamp (λ_{exc} = 365 nm).

mixtures of increasing polarity (see Supporting Information, Figure S63).

Subsequently, a representative member of the ester-substituted aroyl-S,N-ketene acetals, here dye **3l**, was encapsulated into polystyrene particles (PSPs) using a swelling-based staining procedure in a water/THF mixture as described by Behnke et al.[68] This simple staining procedure enables the efficient incorporation of hydrophobic luminophores into the apolar PS matrix of noncrosslinked PSPs with different surface functionalities without requiring the introduction of a functional group into the fluorophores as a prerequisite for the covalent attachment to the polymer matrix. Excitation of **3l**-stained PSPs at 397 nm, revealed a blue shift in the emission maximum of the encapsulated dye relative to the fluorescence spectra of the aggregated state observed in water/THF mixture. This blue shift is attributed to a less polar microenvironment of the dye molecules within the PS matrix compared to the dye aggregates in water/ethanol mixtures. Quantum yield measurements revealed a Φ_f of 30% of the PSP-encapsulated dye (Figure 5). The observed enhancement in emission efficiency is attributed to the rigidification of the dye within the polystyrene network, which restricts intramolecular motions and thereby reduces nonradiative decay pathways.

3. Conclusion

Ester-substituted aroyl-*S*,*N*-ketene acetals were readily obtained in a sequential one-pot desymmetrizing double acylation of di(hetero)aroyl dichlorides with alcohols and 2-methyl *N*-benzyl thiazolium salts in a three-component fashion under mild conditions and in good yields. The key to this selective transformation is the difference in nucleophilicity of the alcohols and the in situ generated *S*,*N*-ketene acetals. The obtained library of the ester-substituted aroyl-*S*,*N*-ketene acetals expectedly displays very similar absorption characteristics, which are dominated by the charge-transfer transition along the merocyanine dipole axis. In contrast, the solid-state emission of the dyes and their AIE characteristics studied in water/ethanol solvent mixtures of varying water content, and hence polarity, are considerably affected by the nature of the alcohol component. Parameters controlled by the alcohol moiety include the water fraction at which maximum AIE effects are observed as well as the emission color and fluorescence efficiency of the resulting dye aggregates. The fluorescence properties of these novel dyes can be also enhanced by encapsulation into PSPs as exemplarily demonstrated for dye **3l**, revealing a fluorescence quantum yield (Φ_f) of 30% in the apolar and relatively rigid polymer network compared to maximally 11% of the dye aggregates in the water/ethanol mixtures. The presented novel synthetic approach now opens numerous alleys to functionalized aroyl-*S*,*N*-ketene acetals. Studies directed to the methodological expansion as well as to new functionality decorated AIEgens are currently underway, including the further systematic development of amide-substituted aroyl-*S*,*N*-ketene acetals (see Supporting Information, Figure S63).

Supporting Information

The authors have cited additional references within the Supporting Information.[57,61–66,69]

Acknowledgments

The authors are grateful to the Deutsche Forschungsgemeinschaft DFG (Mu 1088/9–1; RE 1203/45–1) and the Fonds der Chemischen Industrie for financial support. We thank the CeMSA@HHU (Center for Molecular and Structural Analytics @ Heinrich Heine University) for recording mass spectrometric and NMR spectroscopic data.

Open access funding enabled and organized by Projekt DEAL.

Conflict of Interest

The authors declare no conflicts of interest.

Data Availability Statement

The data that support the findings of this study are available in the supplementary material of this article.

Keywords: acylation · aggregation-induced emission · merocyanines · multicomponent reactions · solid-state emission

[1] J. Griffiths, *Chimia* **1991**, *45*, 304.
[2] T. J. J. Müller, U. H. F. Bunz, eds. In *Functional Organic Materials Syntheses, Strategies and Applications*, WILEY-VCH, Weinheim **2007**.
[3] M. Grätzel, *Nature* **2001**, *414*, 338.
[4] A. Mishra, M. K. R. Fischer, P. Bäuerle, *Angew. Chem. Int. Ed.* **2009**, *48*, 2474.
[5] Z. R. Li, in *Organic Light-Emitting Materials and Devices*, CRC Press, Boca Raton, USA **2015**.
[6] N. T. Kalyani, S. Dhoble, *Sust. Energ. Rev.* **2012**, *16*, 2696.
[7] K. Müllen, U. Scherf, in *Organic Light Emitting Devices: Synthesis, Properties and Applications*, John Wiley & Sons, **2006**.
[8] J.-S. Park, H. Chae, H. K. Chung, S. Lee, *Semicond. Sci. Technol.* **2011**, *26*, 034001.
[9] L. Torsi, M. Magliulo, K. Manoli, G. Palazzo, *Chem. Soc. Rev.* **2013**, *42*, 8612.
[10] I. Kymissis, in *Organic Field Effect Transistors: Theory, Fabrication and Characterization*, Springer Science & Business Media, **2008**.
[11] D. Nilsson, T. Kugler, P.-O. Svensson, M. Berggren, *Sens. Actuators B Chem.* **2002**, *86*, 193.
[12] C.-T. Chen, H. Wagner, W. C. Still, *Science* **1998**, *279*, 851.
[13] E. Kim, S. B. Park, *Chem. Asian J.* **2009**, *4*, 1646.
[14] C. W. Cairo, J. A. Key, C. Sadek, *Curr. Opin. Chem. Biol.* **2010**, *14*, 57.
[15] H.-A. Wagenknecht, *Ann. Ny. Acad. Sci.* **2008**, *1130*, 122.
[16] N. A. Romero, D. A. Nicewicz, *Chem. Rev.* **2016**, *116*, 10075.
[17] Q.-Q. Zhou, Y.-Q. Zou, L.-Q. Lu, W.-J. Xiao, *Angew. Chem. Int. Ed.* **2019**, *58*, 1586.
[18] S. Dutta, J. E. Erchinger, F. Strieth-Kalthoff, R. Kleinmans, F. Glorius, *Chem. Soc. Rev.* **2024**, *53*, 1068.
[19] C. A. Briehn, P. Bäuerle, *Chem. Commun.* **2002**, *2*, 1015.
[20] N. S. Finney, *Curr. Opin. Chem. Biol.* **2006**, *10*, 238.
[21] M. Vendrell, D. Zhai, J. C. Er, Y.-T. Chang, *Chem. Rev.* **2012**, *112*, 4391.
[22] F. de Moliner, N. Kielland, R. Lavilla, M. Vendrell, *Angew. Chem. Int. Ed.* **2017**, *56*, 3758.
[23] M. L. Alfieri, L. Panzella, O. Crescenzi, A.l. Napolitano, M. d'Ischia, *Eur. J. Org. Chem.* **2021**, *2021*, 2982.
[24] H. Xin, B. Hou, X. Gao, *Acc. Chem. Res.* **2021**, *54*, 1737.
[25] L. Zhang, C. Wang, Y. Li, H. Wang, K. Sun, S. Lu, Y. Wang, S. Jing, T. Cordes, *Angew. Chem. Int. Ed.* **2025**, *64*, e202415627.
[26] T. J. J. Müller, in *Science of Synthesis: Multicomponent Reactions Vol. 1: General Discussion and Reactions Involving a Carbonyl Compound as Electrophilic Component*, Georg Thieme Verlag, **2014**.
[27] R. Roszak, L. Gadina, A. Wołos, A. Makkawi, B. Mikulak-Klucznik, Y. Bilgi, K. Molga, P. Gołębiowska, O. Popik, T. Klucznik, S. Szymkuć, M. Moskal, S. Baś, R. Frydrych, J. Mlynarski, O. Vakuliuk, D. T. Gryko, B. A. Grzybowski, *Nature Commun* **2024**, *15*, 10285.
[28] T. J. J. Müller, in *Functional Organic Materials. Syntheses, Strategies, and Applications*, (Eds: T. J. J. Müller, U. H. F. Bunz), Wiley-VCH Verlag GmbH & Co. KGaA, Weinheim **2007**, pp. 179–223.
[29] T. J. J. Müller, D. M. D'Souza, *Pure Appl. Chem.* **2008**, *80*, 609.
[30] L. Levi, T. J. J. Müller, *Chem. Soc. Rev.* **2016**, *45*, 2825.
[31] L. Levi, T. J. J. Müller, *Eur. J. Org. Chem.* **2016**, 2907.
[32] R. O. Rocha, M. O. Rodrigues, B. A. D. Neto, *ACS Omega* **2020**, *5*, 972.
[33] L. Brandner, T. J. J. Müller, *Front. Chem.* **2023**, *11*, 1124209.
[34] B. A. D. Neto, J. E. P. Sorto, A. A. M. Lapis, F. Machado, *Methods* **2023**, *220*, 142.
[35] Y. Hong, J. W. Lam, B. Z. Tang, *Chem. Commun.* **2009**, 4332.
[36] Y. Hong, J. W. Lam, B. Z. Tang, *Chem. Soc. Rev.* **2011**, *40*, 5361.
[37] R. Hu, N. L. C. Leung, B. Z. Tang, *Chem. Soc. Rev.* **2014**, *43*, 4494.
[38] P. Mazumdar, S. Maity, M. Shyamal, D. Das, G. P. Sahoo, A. Misra, *Phys. Chem. Chem. Phys.* **2016**, *18*, 7055.
[39] J. Mei, N. L. C. Leung, R. T. K. Kwok, J. W. Y. Lam, B. Z. Tang, *Chem. Rev.* **2015**, *115*, 11718.
[40] F. K. Merkt, T. J. J. Müller, *Isr. J. Chem.* **2018**, *58*, 889.
[41] L. Biesen, N. Nirmalananthan-Budau, K. Hoffmann, U. Resch-Genger, T. J. J. Müller, *Angew. Chem. Int. Ed.* **2020**, *59*, 10037.
[42] L. Biesen, D. Woschko, C. Janiak, T. J. J. Müller, *Chem. Eur. J.* **2022**, *28*, e202202579.
[43] L. Biesen, T. J. J. Müller, *Chem. Eur. J.* **2023**, *29*, e202302067.
[44] Y. Zhu, G. B. Schuster, *J. Am. Chem. Soc.* **1993**, *115*, 2190.
[45] M. Kamata, M.; G. B. Schuster, *J. Org. Chem.* **1993**, *58*, 5323.
[46] T. De Paulis, K. Hemstapat, Y. Chen, Y. Zhang, S. Saleh, D. Alagille, R. M. Baldwin, G. D. Tamagnan, P. J. Conn, *J. Med. Chem.* **2006**, *49*, 3332.
[47] C.-Y. Cuilleron, E. Mappus, M. G. Forest, *Steroids* **1981**, *38*, 607.
[48] L. Zhang, J. Dong, X. Xu, Q. Liu, *Chem. Rev.* **2016**, *116*, 287.
[49] Z. Wang, in *Comprehensive Organic Name Reactions and Reagents*, John Wiley & Sons, **2010**, pp. 967–970.
[50] H. Mayr, B. Kempf, A. R. Ofial, *Acc. Chem. Res.* **2003**, *36*, 66.
[51] H. Mayr, A. R. Ofial, *Pure Appl. Chem.* **2005**, *77*, 1807.
[52] H. Mayr, A. R. Ofial, *J. Phys. Org. Chem.* **2008**, *21*, 584.
[53] Z. Li, P. Ji, J.-P. Cheng, *J. Org. Chem.* **2021**, *86*, 2974.
[54] B. Maji, M. Horn, H. Mayr, *Angew. Chem. Int. Ed.* **2012**, *51*, 6231.
[55] B. Maji, H. Mayr, *Angew. Chem. Int. Ed.* **2012**, *51*, 10408.
[56] J. Ammer, M. Baidya, S. Kobayashi, H. Mayr, *J. Phys. Org. Chem.* **2010**, *23*, 1029.
[57] G. H. Alt, *J. Org. Chem.* **1968**, *33*, 2858.
[58] J. Krenzer, T. J. J. Müller, *Beilstein J. Org. Chem.* **2025**, *21*, 1201.
[59] R. Davis, N. S. Saleesh Kumar, S. Abraham, C. H. Suresh, N. P. Rath, N. Tamaoki, S. Das, *J. Phys. Chem. C* **2008**, *112*, 2137.
[60] X. He, A. C. Benniston, H. Saarenpää, H. Lemmetyinen, N. V. Tkachenko, U. BaischChem, *Sci.* **2015**, *6*, 3525.
[61] M. J. Frisch, G. W. Trucks, H. B. Schlegel, G. E. Scuseria; M. A. Robb, J. R. Cheeseman, G. Scalmani, V. Barone; G. A. Petersson, H. X. Nakatsuji, M. C. Li, A. V. Marenich, J. Bloino, B. G. Janesko, R. Gomperts, B. Mennucci, H. P. Hratchian, J. V. Ortiz, A. F. Izmaylov, J. L. Sonnenberg, D. Williams-Young, F. Ding, F. Lipparini, F. Egidi, J. Goings, B. Peng, A. Petrone, T. Henderson, D. Ranasinghe, V. G. Zakrzewski, J. Gao, N. Rega, G. Zheng, W. Liang, M. Hada, M. Ehara, K. Toyota, R. Fukuda, J. Hasegawa, M. Ishida, T. Nakajima, Y. Honda, O. Kitao, H. Nakai, T. Vreven, K. Throssell, J. A. Montgomery, J. E. Peralta, F. Ogliaro, M. J. Bearpark, J. J. Heyd, E. N. Brothers, K. N. Kudin, V. N. Staroverov, T. A. Keith, R. Kobayashi, J. Normand, K. Raghavachari, A. P. Rendell, J. C. Burant, S. S. Iyengar, J. Tomasi, M. Cossi, J. M. Millam, M. Klene, C. Adamo, R. Cammi, J. W. Ochterski, R. L. Martin, K. Morokuma, O. Farkas, J. B. Foresman, D. J. Fox, in *Gaussian 16, Revision A.03*; Gaussian Inc., **2016**.
[62] A. D. Becke, *J. Chem. Phys.* **1993**, *98*, 5648.
[63] A. D. Becke, *J. Chem. Phys.* **1993**, *98*, 1372.
[64] C. Lee, W. Yang, R. G. Parr, *Phys. Rev. B* **1988**, *37*, 785.
[65] R. Krishnan, J. S. Binkley, R. Seeger, J. A. Pople, *J. Chem. Phys.* **1980**, *72*, 650.
[66] G. Scalmani, M. J. Frisch, *J. Chem. Phys.* **2010**, *132*, 114110.
[67] An ethanol stock solution of chromophore **3** is prepared and an aliquot is transferred to a 10 mL volumetric flask before adding the corresponding volume of water/ethanol mixture. For insuring ideal mixing and for excluding coagulation as far as possible, the mixtures are treated in an ultrasonic bath for about 5 min before measurement. The fluorescence spectra of the aggregate are then recorded, starting with the mixture with the highest water content.
[68] T. Behnke, C. Würth, E.-M. Laux, K. Hoffmann, U. Resch-Genger, *Dyes Pigm.* **2012**, *94*, 247.
[69] G. Höfle, W. Steglich, H. Vorbrüggen, *Angew. Chem. Int. Ed.* **1978**, *17*, 569.

Manuscript received: June 20, 2025
Revised manuscript received: August 25, 2025
Version of record online: September 4, 2025